REFERENCES

[1] F. C. Rossol, *IEEE Trans. Magn.*, vol. MAG-7, pp. 142-145, March 1971.
[2] T. Kobayashi, P. K. George, and F. B. Humphrey, *IEEE Trans. Magn.*, vol. MAG-12, pp. 202-208, May 1976.
[3] V. Speriosu, Y. D. Rosenthal, F. B. Humphrey, and T. Kobayashi, *IEEE Trans. Magn.*, vol. MAG-15, pp. 875-879, Jan. 1979.
[4] Y. S. Lin, G. S. Almasi, and G. E. Keefe, *IEEE Trans. Magn.*, vol. MAG-13, pp. 1744-1764, Nov. 1977.
[5] —, *J. Appl. Phys.*, vol. 48, pp. 5201-5208, Dec. 1977.
[6] Y. S. Lin, G. S. Almasi, D. B. Dove, G. E. Keefe, and C. C. Shir, *J. Appl. Phys.*, vol. 50, pp. 2258-2260, March 1979.
[7] I. L. Sanders and M. H. Kryder, *J. Appl Phys.*, vol. 50, pp. 2252-2257, March 1979.
[8] M. H. Kryder and A. Deutsch, *SPIE*, vol. 94, High Speed Optical Techniques, pp. 49-57, 1976.
[9] R. Wolfe and T. J. Nelson, paper 11-1, presented at 1978 INTERMAG Conf., Florence, Italy.
[10] Y. S. Lin, D. B. Dove, S. Schwarzl, and C. C. Shir, *IEEE Trans. Magn.*, vol. MAG-14, pp. 494-499, Sept. 1978.
[11] B. E. Argyle, M. H. Kryder, R. E. Mundie, and J. C. Slonczewski, *IEEE Trans. Magn.*, vol. MAG-14, pp. 593-595 Sept. 1978.
[12] G. S. Almasi (private communication).

Dynamic Behavior of Domain Walls in Double Layer Self-Biasing Bubble Garnet Films

JAN J. ZEBROWSKI AND FLOYD B. HUMPHREY, FELLOW, IEEE

Abstract—**Radial expansion of bubbles and gradient bubble propagation experiments were conducted in a double layer garnet film with perpendicular anisotropy in both layers. Implanted and as-grown samples are compared. In radial expansion the side walls of the bubble exhibit a linear mobility much lower than calculated from $\gamma\Delta/\alpha$. Saturation occurs at high drives (35 Oe). At drives above 50 Oe the saturation velocity of 27 m/s occurs only in the first 120 ns of the motion. After that the velocity drops to 17.5 m/s still independent of drive. This break in velocity does not occur in implanted samples, where the saturation velocity depends on implantation conditions. In gradient propagation saturation occurs at fields an order of magnitude smaller. The saturation velocity is independent of implantation, but overshoot depends strongly on it. No creep was detected. The 180° head-on domain wall between the two layers is found to have little effect on the dynamics of the side walls of the bubble. The motion of the head-on wall is also investigated and its velocity estimated. This head-on wall exhibits a linear mobility and a saturation velocity at high drives.**

I. INTRODUCTION

THE STATIC properties of magnetic bubble domains in double layer garnet films with perpendicular anisotropy have been investigated in recent years. Interest centered around the possibility of obtaining films in which bubble domains were stable without any external applied magnetic field. De Bonte [1] used a variational model to calculate the stability region of a bubble capped with a head-on wall. This wall, which is the effect of an exchange coupling between the top and the bottom layer, was assumed to have the same energy density as the Bloch wall. It creates an effective bias acting on the bubble. Uchishiba *et al.* investigated the biasing effect by growing films of different compositions [2], [3]. Device structures were created on these films and operational margins measured. Temperature stable self-biasing structures were also examined [4]. The results indicate that the general trend of De Bonte's predictions are correct but the details are difficult to assess because of the complicated nature of device structure. Recently, Kobayashi [5] in an attempt to improve the model of De Bonte also investigated self-biasing structures. He assumed that the capping wall has the same energy density as a 180° infinite head-on wall and derived a formula for the effective biasing field due to this wall. A more detailed model of the capping wall was presented by Menz *et al.* [6]. They assumed the specific structure of this capping wall to have cylindrical symmetry with a Bloch point in the center. This model was consistent with observed state switching, however, wall dynamics was not included.

The purpose of this paper is to investigate the dynamic behavior of domain walls in double layer self-biased films. Radial expansion experiments and gradient propagation are made to characterize the motion of the capped bubble. The head-on wall is moved in a separate experiment and its velocity is estimated.

II. DOMAIN STATICS IN DOUBLE-LAYER FILMS

Consider a double layer film in which one layer has a high anisotropy normal to the plane and is totally saturated in one direction; whereas, the other layer has the same saturation

Manuscript received February 12, 1979; revised June 21, 1979. This work was supported by the National Science Foundation, Division of Materials Research, under Grant DMR-77-24024.

J. J. Zebrowski is with the California Institute of Technology, Pasadena, CA 91125, on leave from the Institute of Physics, Warsaw Technical University, Warszawa, Poland.

F. B. Humphrey is with the California Institute of Technology, Pasadena, CA 91125.

0018-9464/79/1100-1915$00.75

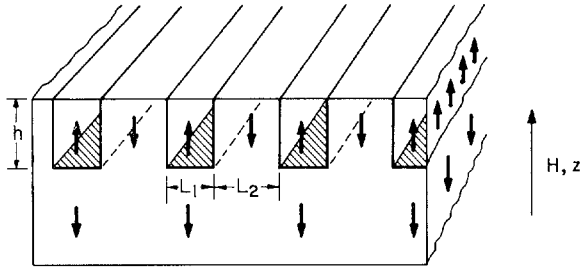

Fig. 1. Stripe domain structure in double layer film.

magnetization and a lower anisotropy with nucleated walls so that an equilibrium domain structure can be expected. A schematic of such a structure can be seen in Fig. 1 for a condition with no external applied field. It can be seen that two kinds of stripe domains exist: those magnetized parallel to the second layer and those magnetized antiparallel. Between every other stripe in the upper layer and the saturated lower layer, a 180° head-on wall is present. The energy per unit area E_T of a parallel stripe array relative to the homogeneously magnetized state, in the direction of the applied field, can be given in the form:

$$E_T = \frac{2h}{L_1 + L_2}\sigma_w + \frac{L_1}{L_1 + L_2}\sigma_c + h\left(1 - \frac{L_1}{L_1 + L_2} + \frac{L_2}{L_1 + L_2}\right)HM_s + E_D$$

where σ_w is the side wall energy density, σ_c is the energy density of the 180° capping wall, H is the applied field, M_S is the saturation magnetization the same in both layers, E_D is the demagnetizing energy of the stripe array (per unit area), L_1 and L_2 are the stripe widths as shown in the figure, and h is the thickness of the layer with the domain structure. Normalizing the total energy E_T by $4\pi M_s^2 h$ and introducing the definitions $x = (L_1 - L_2)/(L_1 + L_2)$ and $y = 2h/(L_1 + L_2)$

$$\tilde{E}_T = y\frac{l}{h} + (1 + x)\left(\frac{l_c}{2h}\right) + (1 - x)\frac{H}{4\pi M_s} + \tilde{E}_D$$

and $l = \sigma_w/4\pi M_s^2$, $l_c = \sigma_c/4\pi M_s^2$, and $\tilde{E}_D = E_D/4\pi M_s^2 h$. This total energy of a stripe array in a double layer film differs from the energy of a similar array in a single-layer system by an additional term $l_c/2h$. This term can be treated as due to an effective field due to the wall energy of the 180° capping wall. For this reason the saturated (lower) layer will be called the biasing layer. The effective field H_{eff} causes stripes to be of unequal width at zero bias field. Applying a field to make the stripes equal in width should just cancel H_{eff} and therefore be a convenient measure for it.

Bubbles in the double-layer film will be of two kinds. The "capped" bubble with the 180° capping wall seen illustrated in Fig. 2(a) and the "skirted" bubble as shown in Fig. 2(b). Just as for stripes, the effective field due to the capping wall should influence the bubble, so that the force equation for bubbles in the material should be

$$\frac{l}{h} + \frac{d}{h}\left(\frac{H}{4\pi M_s} \pm \frac{H_{\text{eff}}}{4\pi M_s}\right) - F\left(\frac{d}{h}\right) = 0$$

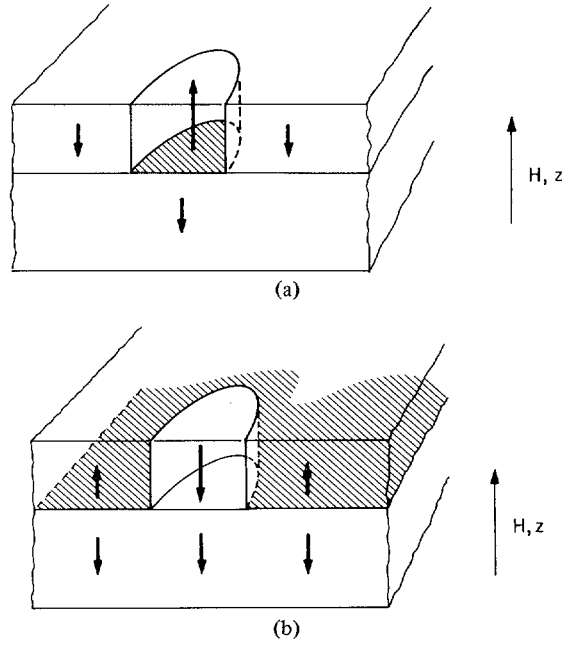

Fig. 2. Two possible bubble domain structures in double layer films. (a) Capped bubble. (b) Skirted bubble.

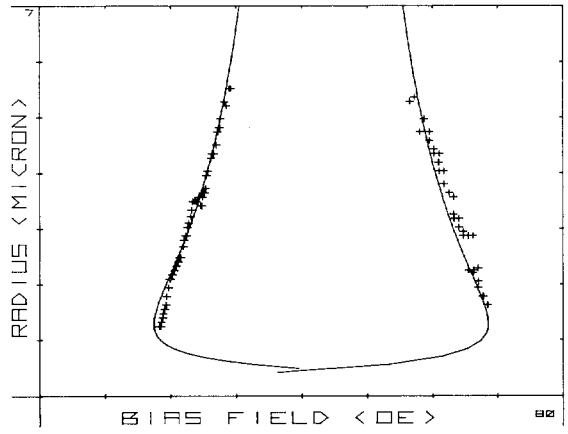

Fig. 3. Bubble domain radius as function of bias field. Solid curve-theory, +–experimental data.

where d is the bubble diameter, $F(d/h)$ is the standard magnetostatic bubble force function and "+" is for the capped bubble. The radius as a function of external applied field normal to the film can be seen in Fig. 3. The left-hand solid curve is for the capped bubble while the right-hand solid curve is for the skirted bubble. The experimental data that is shown in the figure will be discussed later.

III. The Experiment

Transient pictures of bubble domains were taken using a sampling optical microscope system described in detail elsewhere [7]. In this system a flowing nitrogen laser and dye cell are used to produce a real image of the bubble domains with a 10 ns exposure time. The laser flash is synchronized with the bias field pulse or the gradient field pulse. The relative time between the laser flash and the magnetic field pulse can be controlled manually or automatically incremented after each flash. The bubble response to the pulse is determined by taking a se-

ries of pictures with an incremental delay either 0.2 ns or 5 ns, depending on the experimental situation. A video recorder was used to record the individual frames. The size or position of the bubble was measured in each television frame and plotted as a function of time to obtain the velocity under various drive conditions. Due to the small thickness of the bubble layer of the sample, the polarizers in the optical system were crossed for a light background. This made the dark bubble more visible for the measurement of bubble position or size. In the capping wall motion experiment, however, the polarizers were perfectly crossed in order to make small changes in contrast more visible.

Pulse bias fields were obtained using a small, ten-turn pancake coil placed underneath the sample at the bubble layer side. Bias field pulses up to 100 Oe were available and typically 150 to 300 ns long. The rise time varied between 15 and 25 ns depending on the number of pulses used simultaneously. In capping wall motion experiments the same pancake coil was used. The bubble was first expanded with a 52-Oe, 200-ns long pulse and immediately afterwards, a collapse pulse was applied. This pulse lasted until about 10 ns after the laser flash. In this way the bubble could relax back to static equilibrium size immediately after the picture was taken.

Gradient propagation experiments were made using two parallel thin film conductors 1 μm $\times$ 30 μm with center-to-center spacing of 90 μm. The gradient pulses of up to 7.6 Oe/μm were 150 to 300 ns long. Spacing between the sample surface and the conductors was less than 10 μm. Compensation was provided by applying a ramp top pedestal pulse to the ten-turn pancake coil placed underneath the conductors. Creep was investigated by applying 10 uniform 10-Oe bias field pulses approximately 100 ns in length. After each propagation, the bubble was repositioned by a series of 100 ns gradient pulses just above the coercive field. Initial positions were kept within 1.5 μm of each other and bubbles were propagated in the direction away from the center line towards one of the conductors.

The sample used was a double layer garnet sample with a bubble layer of nominal composition $Y_{2.6}Sm_{0.4}Ga_{1.9}Fe_{3.1}O_{12}$. The magnetic characteristics were $4\pi M_s = 140$ G, $l = 0.63$ μm, $h = 1.4$ μm, $H_{\text{eff}} = 43$ Oe, and, as measured by ferromagnetic resonance, $H_k = 1500$ Oe, $\alpha = 0.158$, and $\gamma = 1.75 \times 10^7$ 1/s Oe. The bias layer had the nominal composition $Eu_{0.9}Er_{2.1}\cdot Ga_{0.7}Fe_{4.3}O_{12}$ with $4\pi M_s = 140$ G. The anisotropy was undoubtedly high, however, the line width in ferromagnetic resonance was large (estimated $\alpha = 0.85$) and it could not be measured. Two chips of this sample were implanted with 1×10^{14} Ne^+/cm^2 at 50 keV and with 2×10^{14} at 100 keV, respectively.

IV. Results

The dynamic character of the capped bubble was obtained using free bubble radial expansion. The radius of the capped bubble as a function of time is shown in Fig. 4. A 200-ns long 36.6-Oe bias pulse was applied at $t = 50$ ns in the direction tending to increase the bias field. It can be seen that the bubble expands essentially linearly with time while the pulse is applied. At the end of the pulse, at $t = 250$ ns, the bubble starts returning immediately toward its equilibrium size. No overshoot can be seen.

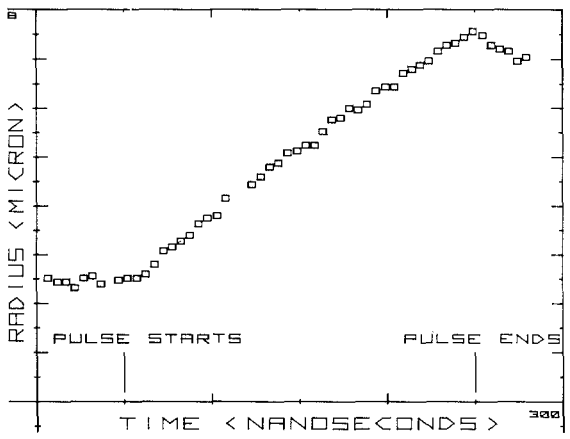

Fig. 4. Bubble domain radius as a function of time under the influence of a 36.6-Oe, 200-ns long expansion pulse.

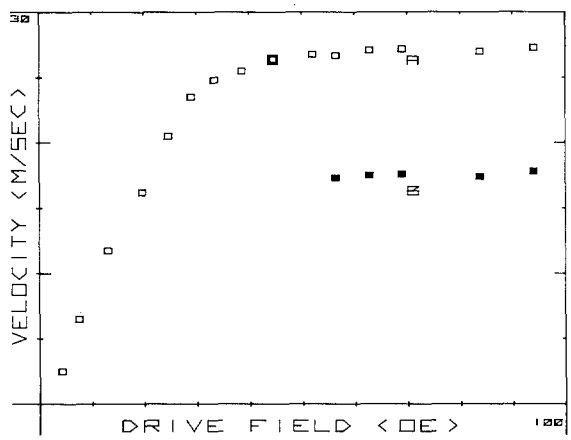

Fig. 5. Velocity of the side walls of the bubble in radial expansion as a function of drive. Curve A: initial velocity; Curve B: final velocity after the break.

Wall velocity in radial expansion can be obtained from the radius as a function of drive data. The average velocity during the first 200 ns as a function of the applied pulse field is shown in Fig. 5 for the as-grown sample. A least-squares fit of the wall position as a function of time is used to determine the slope and hence the average velocity during this time interval. At higher drives, a very significant break appears in the slope of the radius as a function of time curve. Two fits are made to determine the initial velocity and the velocity above the break. The radius versus time is sufficiently linear to make the error in velocity typically ± 0.5 m/s and always less than ± 1 m/s. Looking at curve A, it can be seen that the velocity increases linearly with drive up to about 30 Oe with a slope of 0.85 m/Oe s. Above 50 Oe, the velocity was 27 m/s essentially independent of drive. For drive field pulses less than 52 Oe, the velocity was nearly constant during the entire 200 ns pulse. For higher drives, however, after 120 ns the velocity drops abruptly from 26 m/s to 17.5 m/s. This lower velocity is shown by curve B in Fig. 5. In this region, the initial velocity (curve A) is still independent of drive and seems unaffected by the change in mechanism.

For implanted samples, the velocity as a function of drive has essentially the same shape as curve A in Fig. 5. Implantation, however, removes the lower branch (curve B) of the ve-

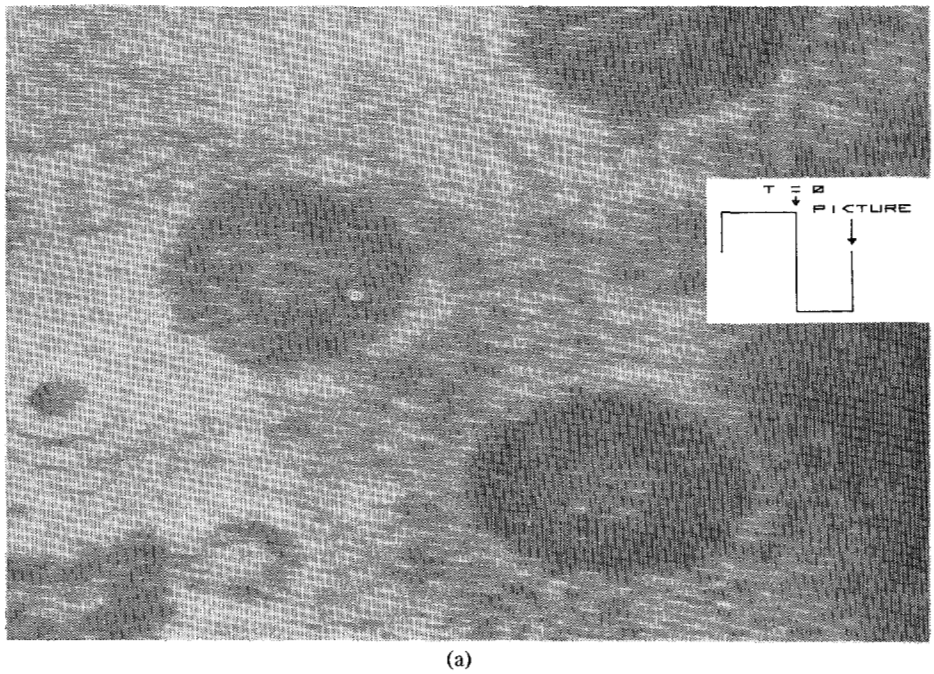

(a)

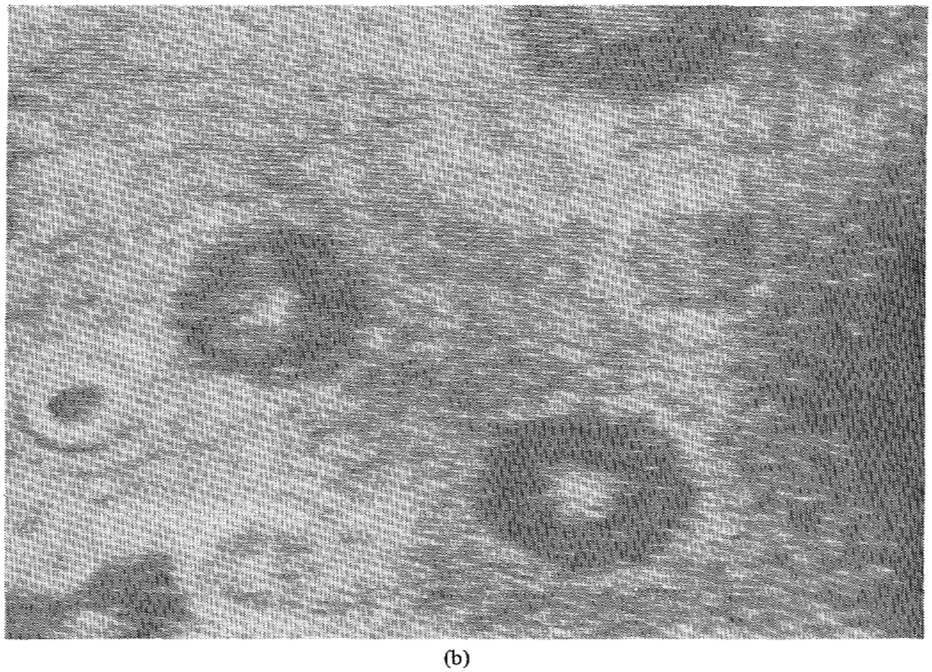

(b)

Fig. 6. Capping wall motion after the application of the 48-Oe collapse pulse. (a) 80 ns. (b) 125 ns. (c) 170 ns.

locity versus drive relation. For the sample implanted at 50 keV and 1×10^{14} Ne^+/cm^2 the saturation velocity was 24 m/s with a mobility of 0.65 m/Oe s. Saturation velocity in the sample implanted at 100 keV and 2×10^{14} Ne^+/cm^2 was 30 m/s and the mobility was 0.8 m/Oe s.

Skirted bubbles were also investigated using radial expansion. In the range of fields below 50 Oe, the velocities measured were the same as for the capped bubble within experimental error. The linear mobility was 0.7 m/Oe s and saturation velocity 27 m/s. Above 50 Oe spontaneous domain nucleation takes place as portions of the capping wall (the bubble "skirt") are lifted from the interface and subsequently punch through the outer surface creating new bubbles.

The head-on wall within the capped bubble can be moved from the bias layer interface to the film surface by applying a collapse pulse. To expand the range of collapse fields in which this motion is observable before the domain shrinks and collapses, the bubble is first expanded by a 200 ns, 50 Oe pulse to a large bubble of 7 μm in radius. Immediately afterwards, the collapse pulse was applied and a picture taken at various times during this pulse. A typical picture can be seen in Fig. 6 with pulse sequence indicated in the insert. For these pictures, the polarizers were crossed so that the stable bubble was a dark spot on a light background. Fig. 6(a) shows the bubble 80 ns after the application of the collapse pulse. It can be seen that as the domain contracted a cloudy spot appeared in its

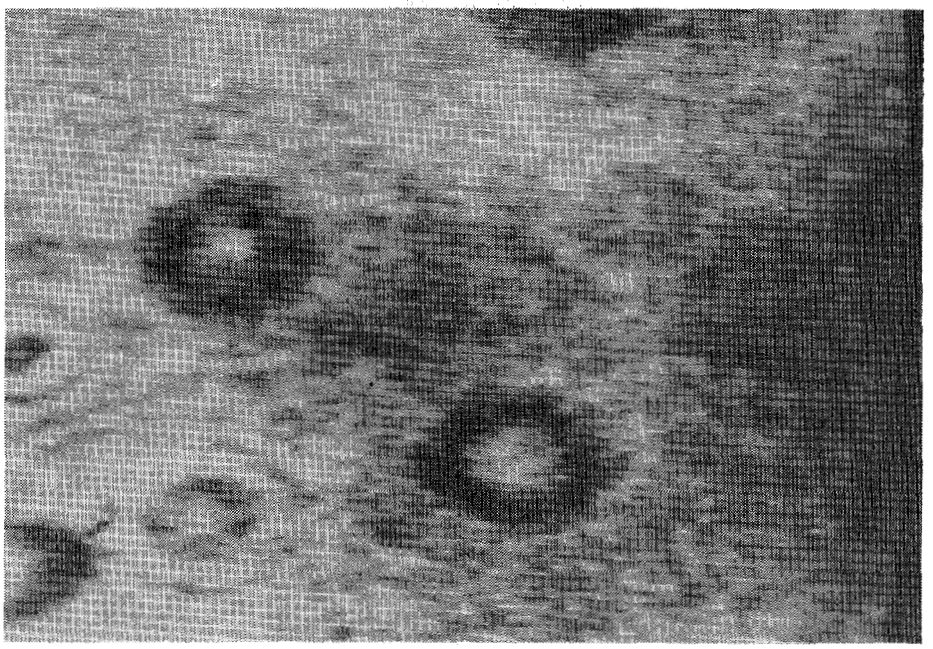

(c)

Fig. 6. *(Continued.)*

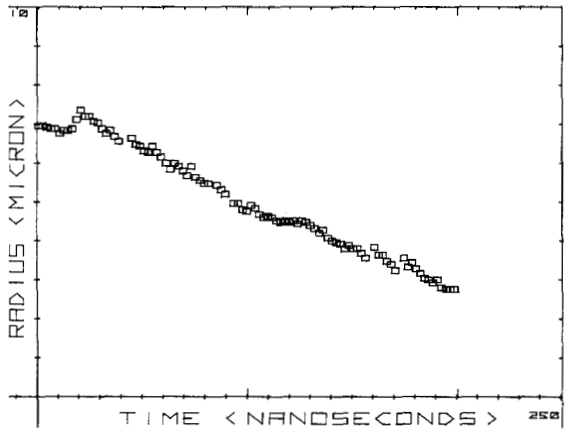

Fig. 7. Radius as function of time of bubble after application of 65 Oe collapse pulse in capping wall motion experiment.

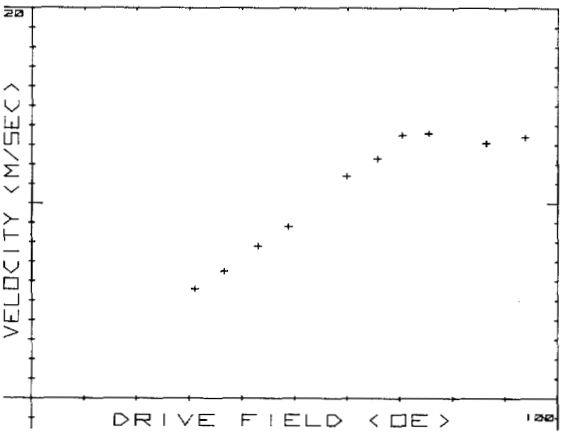

Fig. 8. Velocity in capping wall motion as function of pulse height.

center. This spot developed the same contrast as the outside of the domain by 125 ns after the onset of the collapse pulse as seen in Fig. 6(b). Finally, a well-defined ring bubble was visible as shown in Fig. 6(c) taken 170 ns after the beginning of the collapse pulse. This ring domain is not statically stable and after the end of the collapse pulse the domain reverts to its statically stable capped bubble state.

The radius of the collapsing domain as a function of time after the end of the expanding pulse is shown in Fig. 7. A 65-Oe collapse pulse was used. It can be seen that a rather rapid but small increase in the radius of the domain is observed at approximately 25 ns after the onset of the collapse pulse. This radius increase is seen in all cases measured. After this initial increase, the radius decreases linearly with time. Since the radius of a ring bubble theoretically should be larger than that of a cylindrical bubble in the same material with the same applied bias field [8], the time at which the bubble attained its maximum radius was assumed to be the beginning of the motion of the capping wall. Unfortunately, punchthrough seems to have no observable effect on the radius so that the end of the motion has to be determined by other means.

The average velocity of the 180° capping wall can be obtained by measuring the time this wall needs to move through the film. The average velocity as a function of pulse height is shown in Fig. 8. The velocity is the thickness of the bubble layer (1.4 μm) divided by the time from the end of the initial radius expansion until in the center of the bubble a spot is visible, which has the same contrast as the outside of the domain. It can be seen that the velocity is linear with pulse height up to 70 Oe and then becomes independent of drive. The velocity extrapolates to zero at approximately 4 Oe. The range of drive fields in which the measurement was conducted was limited on the one side by bubble-bubble interactions during the final phase of expansion and by bubble collapse on the other.

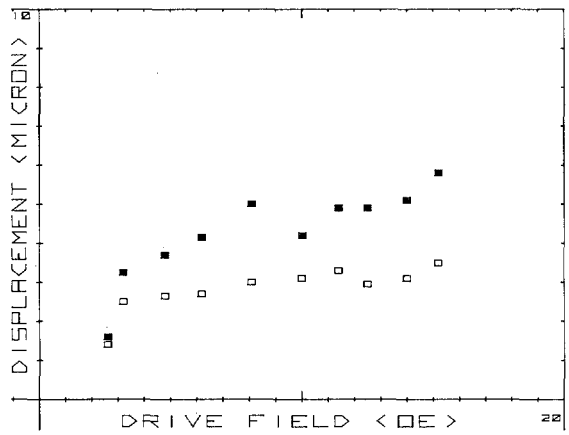

Fig. 9. Displacement in gradient propagation of bubble in the as-grown sample. Driven displacement: open squares; final position: closed squares.

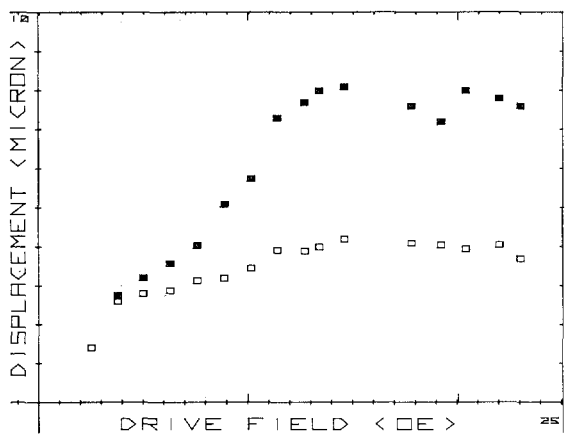

Fig. 10. Displacement in gradient propagation of a bubble in the sample implanted with 2×10^{14} Ne^+/cm^2 at 100 keV. Driven displacement: open squares; final position: closed squares.

Gradient propagation was investigated by taking pictures of the transient bubble during a pulsed gradient field. Overshoot was observed by measuring the position of the bubble long after the end of the pulse. Driven displacement and overshoot as a function of drive for the as-grown sample is presented in Fig. 9. The bubble position at the end of the 250-ns long gradient pulse is shown by open squares and the final position by closed squares. It can be seen that the bubble velocity saturates sharply above 3 Oe drive. At the same drive the first overshoot is visible. No creep [9] was detected. The transient shape of the bubble was triangular. The observed transient shape with the overshoot increasing linearly with drive and the lack of creep indicate that vertical Bloch lines may be generated during the motion but that they are not sustained statically.

For implanted samples, the driven displacement was similar, however, overshoot depended on the implantation dose. Fig. 10 shows displacement (open squares) and (closed squares) final position for the sample implanted with 2×10^{14} Ne^+/cm^2 at 100 keV. It can be seen that the driven displacement is essentially constant above 3 Oe as before. There seems to be a linear region between 3 Oe and 11 Oe, with a very slight slope. Furthermore, overshoot is larger than the as-grown sample and sometimes exceeds driven displacement. Above 11 Oe overshoot is independent of drive. The transient shape is as triangular as in the as-grown sample. No overshoot was detected in a sample implanted at 1×10^{14} Ne^+/cm^2 at 50 keV and the transient shape of bubbles in that sample was elliptical. The character shown here seems to be very sensitive to the implant conditions. Unfortunately, not enough samples were available to obtain more information on this effect.

V. Discussion and Conclusions

The static theory with the value of H_{eff} taken from direct measurement agrees very well with experimental data on the radius as a function of bias field. This can be seen in Fig. 3 where the measured static radius as a function of bias field is plotted with the theoretical curve calculated using the value of $H_{eff} = 43$ Oe measured on stripe domains. The left-hand curve is for the capped bubble and the right-hand curve is for the skirted bubble. The l value used in these calculations was also taken from equilibrium stripe measurements, but was corrected by about 10 percent to fit the slope of the experimental data. The value of $4\pi M_s$ was adjusted so as to fit for both bubble types simultaneously with the value of H_{eff} known from stripe domain measurement and held constant. The effective field can be calculated from a recent model by Kobayashi [5]. In that model the capping wall is assumed to have the same structure as an infinite 180° head-on-wall. The effective field is then shown to be $H_{eff}/4\pi M_s = (l/2h)\sqrt{1 - (1/q)}$, where q is the quality factor of the material. For the material of the sample $H_{eff} = 32$ Oe, i.e., 11 Oe less than the measured value.

Domain wall dynamics in double layer films is complicated in detail. The behavior of the bubble seems to indicate, however, that the double layer film can generally be treated as a single layer structure of the same thickness as the bubble layer but with a built-in bias field equal to the effective field H_{eff}. Both in radial expansion and in gradient propagation the capping wall does not seem to have any noticeable effect on the dynamics of walls. The capping wall itself is seen to move between the surfaces of the bubble layer and exhibits an initial linear mobility and a saturation. From the point of view of dynamics, there seems no reason to believe that bubbles in double layer films will behave any differently in device structures from their single layer counterparts.

Acknowledgment

The authors would like to thank Fujitsu Laboratories for providing the samples. The authors are also very much indebted to the discussions with T. Kobayashi.

References

[1] W. J. De Bonte, "stability of half-bubbles in double-layer films," in *AIP Conf. Proc.* (Magnetism and Magnetic Materials-1972), no. 10, pp. 349-353, 1973.

[2] H. Uchishiba, H. Tominaga, T. Namikata, and S. Sakai, "Internal bias effect of double layer epitaxial garnet films," *IEEE Trans. Magn.*, vol. MAG-9, No. 3, pp. 381-385, Sept. 1973.

[3] H. Uchishiba, H. Tominaga, and T. Namikata, "Self-biasing effect of double layer epitaxial garnet films," *Fujitsu Scientific & Technical.*, pp. 165-188, June 1974.

[4] H. Uchishiba, H. Tominaga, and K. Asama, "Temperature stable

self-biasing bubbles in double layer films," *IEEE Trans. Magn.*, vol. MAG-11, no. 5, pp. 1079–1081, Sept. 1975.
[5] T. Kobayashi, D. M. Meinz, and E. C. Whitcomb, "Self-biased structures for bubble devices," *Digest 1977 Intermag Conf.*
[6] W. Menz, E. B. Moore, and H. L. Hu, "Wall state stability of bubbles in uniaxial double-layer LPE films," *IEEE Trans. Magn.*, vol. MAG-14, no. 5, pp. 599–601, Sept. 1978.
[7] F. B. Humphrey, "Transient bubble domain configuration in garnet materials observed using high speed photography," *IEEE Trans. Magn.*, vol. MAG-11, no. 6, nov. 1975.
[8] F. de Jonge, and W. Druyvesteyn, "Calculations and experiments related to the magnetostatics of bubble domains," *Feskorperprobleme* XII, pp. 531–595, 1972.
[9] K. Ju and F. B. Humphrey, "Gradient propagation, overshoot, and creep in magnetic bubble garnet material," *J. Appl. Phys.*, vol. 48, no. 11, pp. 4656–4665, Nov. 1977.

Statistical Effects in Longevity Measurements on Bubble Memories

JEROLD A. SEITCHIK, MEMBER, IEEE, AND ALEX CLOSSON

Abstract—**A distribution function is presented in closed form which describes the statistical errors expected in longevity slope measurements made on the data loops of a bubble memory. Plots of this function are provided for several common experimental cases. The standard deviation of the distribution function is used to establish how experimental parameters should be selected to minimize statistical error. Limiting cases are examined. Averaging and the problems associated with fitting curves to longevity data points are briefly discussed.**

SHUMATE *et al.* [1], [2] were the first to note that the probability R that a bubble survives t operations is governed by the well-known reliability equation for random failures,

$$R = e^{-t/\tau} \tag{1}$$

where τ is the mean number of operations to failure. They and others [3]–[12] found that τ was strongly dependent on the magnetic bias field chosen for device operation. It is frequently observed that if $\tau = N_A$ at bias H_A then at any other bias H,

$$\tau = N_A 10^{(H-H_A)/\epsilon} \tag{2}$$

where ϵ is a constant commonly called the longevity slope. The upper bias margin is governed by a negative value of ϵ and the lower margin by a positive ϵ. All devices [5], [11] do not exhibit longevity behavior in agreement with (2). We will discuss other observed behaviors in a future work; however, we have not so far found any departures that affect more than relatively minor details of what is presented here.

Because bubble data errors are random in nature, determinations of ϵ made by observing the mean number of steps to failure are subject to statistical error. If the longevity slope of every data loop on a bubble memory device is measured individually, significant variations are seen, particularly in modern day devices which have hundreds of loops. Thus in reviewing multiloop longevity data, it is frequently difficult to decide whether different loops have different slopes or whether they all have the same slope and the measured differences merely portray the statistics. In order to aid in making this distinction, it is useful to compare the measured distribution of slopes with that obtained from the statistical distribution function for slopes obtained by longevity measurements. With this function, we can calculate the expected distribution for measurements made on loops with the same ϵ using only the mean slope of the measured distribution and the measurement parameters.

The longevity slope distribution function (LSDF) also aids in optimizing longevity experiments. It establishes the trade-off between the duration of the longevity measurement and the measurement uncertainty. Alternatively, if the time allocated to the measurement is fixed, it reveals how the measurement parameters should be selected to minimize the uncertainty in the slope determination.

In this paper we present a LSDF for Shumate-type longevity experiments on a group of data loops that have the same longevity slope. Examples of the slope distribution are plotted. Both common and limiting case experimental conditions are examined. Optimization of the measurement procedure is discussed, and the advantages of averaging are reviewed. Some applications are also described.

The Distribution Function

There are a number of ways that longevity experiments can be performed. For example, one can operate a bubble device at fixed biases and determine the number of operations to the first data failure at each bias, or the experimenter can exercise the device for a fixed number of operations and vary the bias between tests until the first data error is encountered. The distribution function for the former experiment may not rigorously describe the latter experiment although it is ex-

Manuscript received February 15, 1979; revised July 10, 1979.
The authors are with the Texas Instruments Incorporated, Dallas, TX 75265.

0018-9464/79/1100-1921$00.75